JOURNAL OF SOLID STATE CHEMISTRY **135,** 228–234 (1998)
ARTICLE NO. SC977629

New Cathode Materials for Rechargeable Lithium Batteries: The 3-D Framework Structures $Li_3Fe_2(XO_4)_3$ (X = P, As)

C. Masquelier,[1] A. K. Padhi, K. S. Nanjundaswamy, and J. B. Goodenough

Center for Materials Science and Engineering, University of Texas at Austin, E.T.C. 9.102, Austin, Texas 78712-1063

Received August 13, 1996; in revised form September 16, 1997; accepted September 18, 1997

Electrochemical insertion of lithium into four $Li_3Fe_2(XO_4)_3$ polymorphs (X = P or As) with 3-D framework structures was carried out in "Li/$LiClO_4$ (PC:DME)/cathode" coin cells. Approximately 2 Li per formula unit could be reversibly inserted into the three different structures, which corresponds to the reduction of all Fe^{3+} to Fe^{2+} between 2.5 and 3.5 V vs lithium. The position of the Fe^{3+}/Fe^{2+} redox couple below the lithium-anode Fermi energy is nearly independent of the structure and of whether X = P or As. There is, however, a clear dependence of (i) the shape of the V_{cc} vs x curves for $Li_{3+x}Fe_2(XO_4)_3$ and (ii) the charge–discharge rate capabilities on the crystal structure of the cathode material. © 1998 Academic Press

Key Words: **Rechargeable lithium batteries; electrochemical insertion; NASICON; ionic conductors; cathodes; iron phosphates; iron arsenates.**

I. INTRODUCTION

Over the past 20 years, intensive research on transition-metal oxides suitable as hosts for a rapid insertion/extraction of alkali ions has led to the development of $LiCoO_2$ (layered rock salt) or $Li[Mn_2]O_4$ (spinel) as cathode materials in rechargeable lithium batteries. Cost, environment, and shelf-life considerations have also prompted a search for alternative cathode systems, among which are the NASICON-related framework structures utilizing the Ti^{4+}/Ti^{3+} or Fe^{3+}/Fe^{2+} redox couples and tetrahedral polyanions $(XO_4)^{2-}$ or $(XO_4)^{3-}$ with X = Mo, W, S, or P (1–9).

NASICON-related materials $Fe_2(XO_4)_3$ (X = Mo, W, S) can be reversibly intercalated with up to 2 lithium ions per formula unit at open-circuit voltages V_{oc} that depend strongly on the chemical nature of the polyanion, which affects the strength of the Fe–O bonds via the inductive effect: a stronger polarization of O^{2-} toward S^{VI} generates a weaker Fe–O bonding, which results in a lowering of the energy of the Fe^{3+}/Fe^{2+} redox couple and hence in a higher open-circuit voltage vs a lithium-metal anode in $Fe_2(SO_4)_3$ (V_{oc} = 3.6 V) (7) than in $Fe_2(MoO_4)_3$ (V_{oc} = 3.0 V) (1, 2). Delmas *et al.* also demonstrated the reversible intercalation of up to 2 lithium or sodium ions per formula unit into the rhombohedral NASICON structures $ATi_2(PO_4)_3$ (A = Li, Na) at V_{oc} = 2.5 V and V_{oc} = 2.2 V vs lithium, respectively, for the Ti^{4+}/Ti^{3+} couple (5, 6).

The electrochemical characteristics, i.e., their behavior as insertion cathode materials in rechargeable lithium batteries, of the two structural modifications of $Fe_2(SO_4)_3$ were recently investigated (7–9). At low current densities ($\sim$0.1 mA/cm^2), both the monoclinic and the rhombohedral forms can reversibly intercalate 1.5 and 1.8 lithium ions per formula unit, respectively, at 3.6 V vs lithium. Additionally, it was shown (8) that the substitution of $(PO_4)^{3-}$ for $(SO_4)^{2-}$, from $Li_xFe_2(SO_4)_3$ to the isotypic $Li_{3+x}Fe_2(PO_4)_3$, results in a decrease of the V_{oc} to 2.8 V vs Li due to the smaller polarization of O^{2-} toward P^V than toward S^{VI}.

More recently, we undertook systematic investigations of the reversible lithium insertion/extraction into/from a large number of polyanion structures ($(SO_4)^{2-}$, $(PO_4)^{3-}$, $(AsO_4)^{3-}$, and $(P_2O_7)^{4-}$) operating on various transition-metal redox couples (Fe^{3+}/Fe^{2+}, Ti^{4+}/Ti^{3+}, V^{3+}/V^{2+}, Nb^{5+}/Nb^{4+}, Nb^{4+}/Nb^{3+}, …) (12–16). Of particular interest are (1) the tuning of the transition-metal redox energies through the inductive effect, i.e., the study of the effect of the nature of the polyanion and of the crystal structure on the energy level of the $M^{n+}/M^{(n-1)+}$ redox couples, and (2) the identification of new cathode materials operating on the Fe^{3+}/Fe^{2+} or Ti^{4+}/Ti^{3+} redox couples. Among these, the olivine Li_xFePO_4 with a flat V_{oc} = 3.5 V vs lithium (12) and the rhombohedral NASICON $Li_{2+x}FeTi(PO_4)_3$ and $Li_{3+x}Fe_2(PO_4)_3$ (13, 14) with a closed-circuit voltage centered at $V \simeq 2.7$ V vs lithium present particularly attractive performances.

[1] To whom correspondence should be addressed at Laboratoire de Chimie des Solides, URA CNRS 446, Bat. 414, Université Paris-XI Orsay, 91405 Orsay Cedex, France. E-mail: Christian.Masquelier@chimsol.u-psud.fr.

0022-4596/98 $25.00

This paper describes the preparation, the characterization, and the electrochemical properties of 3-D framework structures of general formula $Li_3Fe_2(XO_4)_3$ (X = P, As), denoted as LiFeX. Depending on the preparation route and on the nature of the $(XO_4)^{3-}$ polyanion group, three different crystal structures can be obtained (A-*LFX*, B-*LFP*, and C-*LFA*); each can reversibly intercalate approximately 2 lithium ions per formula unit associated with the electrochemical reduction of Fe^{3+} to Fe^{2+}.

II. MATERIALS PREPARATION AND CHARACTERIZATION

The three different forms of $Li_3Fe_2(XO_4)_3$ (X = P, As) considered here were prepared following general routes previously described (17–20). The preparation temperatures and the crystallographic characteristics are summarized in Table 1.

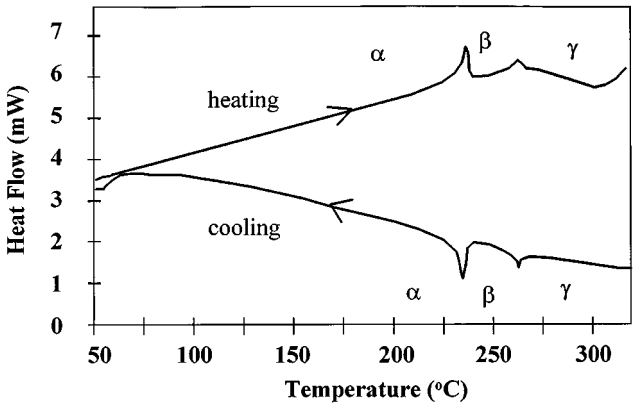

FIG. 1. Differential scanning calorimetry curves recorded between 50 and 325°C for $Li_3Fe_2(PO_4)_3$ (A-*LFP*).

A. Monoclinic $Li_3Fe_2(XO_4)_3$ (A-LFX, X = P, As)

Direct decomposition and solid-state reaction at 930 and 860°C between intimately mixed $LiOH \cdot H_2O$, Fe_2O_3, and $NH_4H_2XO_4$ powders with X = P and As, respectively, lead to $Li_3Fe_2(XO_4)_3$ compositions (A-*LFX*) isotypic with the monoclinic form of $Fe_2(SO_4)_3$ ($P2_1/n$). All the X-ray diffraction peaks for both samples could be indexed in a slightly distorted monoclinic unit cell with lattice parameters (Table 1) very close to previously reported values (18, 20). The monoclinic cell results from a small distortion of the framework from orthorhombic symmetry, due to lithium-ion ordering at room temperature. As previously demonstrated by d'Yvoire *et al.* (18) and Bykov *et al.* (21), differential scanning calorimetry experiments (Fig. 1) show that the monoclinic A-*LFP* (α-form) transforms reversibly to the orthorhombic A-*LFP* (γ-form) upon heating at $T > 270$°C, due to a progressive breaking of the long-range ordering of the Li^+ ions in the interstitial space.

B. "NASICON" $A_3Fe_2(PO_4)_3$ (B-AFP, A = Li, Na)

A second polymorph of chemical composition $Li_3Fe_2(PO_4)_3$, the rhombohedral $R\bar{3}c$ form denoted here B-*LFP*, can be prepared by ionic exchange from the sodium monoclinic analog $Na_3Fe_2(PO_4)_3$ (B-*NFP*) (17, 18). B-*NFP* was first prepared by direct decomposition and solid-state reaction at 920°C of stoichiometric quantities of $NaH_2PO_4 \cdot H_2O$ and Fe_2O_3. The crystal structure of B-*NFP* consists, as for A-*LFP*, of a 3-D framework in which FeO_6 octahedra and PO_4 tetrahedra are connected to each other through all their vertices. In the real NASICON structure, however, the arrangement of MO_6 and XO_4 polyhedra results in a more open structure which allows faster alkali-ion diffusion through bottlenecks of eight-membered rings. As in Hong's $Na_3Zr_2Si_2PO_{12}$ (22), the room-temperature form α-$Na_3Fe_2(PO_4)_3$ presents an ordered distribution of Na^+ ions, which results in a slight distortion of the rhombohedral framework to monoclinic symmetry ($C2/c$) (7).

The substitution of Na by Li by ionic exchange leads to the disordered rhombohedral ($R\bar{3}c$) B-*LFP*. The ionic exchange was performed by three successive immersions of B-*NFP* in an excess (Li/Na ~ 50) of molten $LiNO_3$ at 300°C for about 1 h, separated by extensive rinsing in water. The decrease of the a_{hex} parameter and the important increase of the c_{hex} parameter from B-*NFP* (a = 8.731 Å, c = 21.569 Å in the pseudohexagonal unit cell (17)) to B-*LFP* (Table 1) strongly suggest different alkali-ion distributions. Similar

TABLE 1
Preparation and Crystallographic Data for $A_3Fe_2(XO_4)_3$ Samples (A = Li, Na; X = P, As)

Code	Comp	Prep	a (Å)	b (Å)	c (Å)	β (deg)	V/Z	Space group
A-*LFP*	$Li_3Fe_2(PO_4)_3$	930°C	8.561(3)	8.626(2)	12.026(2)	90.52(3)	222.0	$P2_1/n$
A-*LFA*	$Li_3Fe_2(AsO_4)_3$	860°C	8.620(2)	8.944(2)	12.229(2)	90.78(2)	235.7	$P2_1/n$
B-*NFP*	$Na_3Fe_2(PO_4)_3$	920°C	15.140(1)	8.728(1)	8.805(1)	125.14	237.9	C_2/c
B-*LFP*	$Li_3Fe_2(PO_4)_3$	ionic exchange	8.300(6)		22.53(1)		224.0	$R\bar{3}c$
C-*NFA*	$Na_3Fe_2(AsO_4)_3$	910°C	13.730(6)		18.581(11)		252.8	$R\bar{3}c$
C-*LFA*	$Li_3Fe_2(AsO_4)_3$	ionic exchange	13.639(7)		18.457(11)		247.8	$R\bar{3}c$

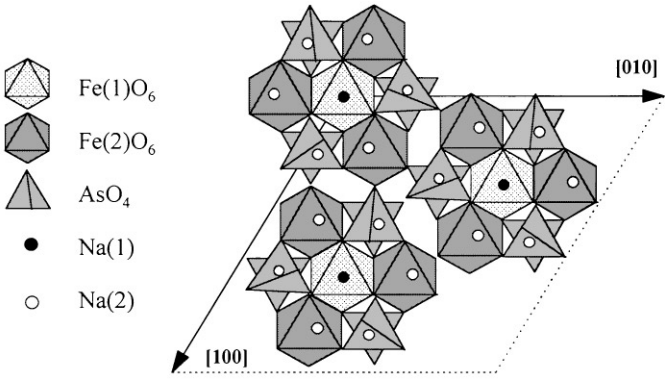

FIG. 2. Partial representation of the structure of II-$Na_3Fe_2(AsO_4)_3$.

observations by Delmas *et al.* (6) for $A_3Ti_2(PO_4)_3$ (A = Li, Na) were attributed to vacant $M(1)$ crystallographic sites along c_{hex}, resulting in a greater electrostatic repulsion between TiO_6 octahedra.

C. $A_3Fe_2(AsO_4)_3$, "Form II" (C-AFA, A = Li, Na)

Ionic exchange was also used to prepare a second polymorph of chemical composition $Li_3Fe_2(AsO_4)_3$, denoted here *C-LFA*, with rhombohedral symmetry ($R\bar{3}c$) and isotypic with II-$Na_3Fe_2(AsO_4)_3$. C-*NFA* was obtained by decomposition and solid-state reaction at 910°C of a stoichiometric mixture of $NaHCO_3$, Fe_2O_3, and $NH_4H_2AsO_4$ followed by quenching to avoid the formation of the garnet I-$Na_3Fe_2(AsO_4)_3$. This original structure, first isolated by Schwarz *et al.* (23) and later characterized by d'Yvoire *et al.* (19, 24), consists of a three-dimensional framework $[Fe_4(AsO_4)_6]_\infty$ made up of Fe_4O_{18} clusters (one central $Fe(1)O_6$ octahedron sharing three edges with three $Fe(2)O_6$ octahedra) linked to AsO_4 tetrahedra (Fig. 2). The sodium ions occupy two independent crystallographic sites: Na(1) is fully occupied and Na(2) has a fractional occupancy of $\tau = \frac{5}{6}$. Mixed-valence Fe^{III}/Fe^{II} crystals of composition $Na_7Fe_4(AsO_4)_6$ were prepared (24), and a recent investigation of their crystal structure (25) demonstrated the chemical reduction of Fe^{3+} to Fe^{2+} on the Fe(1) site associated with the total occupancy of the Na(2) site, leading to the structural formula $Na(1)Na(2)_6Fe^{II}(1)Fe^{III}_3(2)(AsO_4)_6$.

III. ELECTROCHEMICAL STUDY

Electrochemical insertion/extraction of lithium into/from the $Li_3Fe_2(XO_4)_3$ framework structures was performed with Li/$LiClO_4$ (PC:DME)/*LFX* coin cells assembled in an argon-filled glovebox. Hand-rolled cathode sheets were obtained from intimately mixed, fine powders of *LFX* cathode material : acetylene black : PTFE in 70 : 25 : 5 proportions. Pellets of 2-cm^2 area (~100 mg) were cut and pressed between two titanium meshes for the cathodic part of the cell. The cells were discharged and charged at current densities varying between 0.05 and 1 mA/cm^2 (1–20 mA/g) with minimum and maximum cutoff voltages of 2 and 4 V, respectively. Data were monitored and collected with the Arbin Battery Test System (ABTS-BT2020).

A. Monoclinic $Li_{3+x}Fe_2(XO_4)_3$ (A-LFX)

$Li_3Fe_2(PO_4)_3$ (A-*LFP*) has been used as a buffer at ~2.8 V against overdischarge for $Fe_2(SO_4)_3$ (3.6 V) (8). The insertion of lithium into $Li_{3+x}Fe_2(PO_4)_3$ ($0 \le x \le 1.8$) is reversible (Fig. 3a) and would correspond to a discharge capacity of 128 mA h/g if all Fe^{3+} could be reduced to Fe^{2+} ($x = 2$). The observed discharge capacity at relatively low current densities (0.05 mA/cm^2) is 115 mA h/g, corresponding to the insertion of 1.8 lithium ions per formula unit. An increase in the current density to 0.5 mA/cm^2 results in an important decrease of the discharge capacity from 115 to 80 mA h/g (Fig. 3b), but without too big an overvoltage. However, the capacity is partially recovered on returning to a lower current density, which indicates that the loss of capacity may be due to a kinetic effect rather than to a breaking of electric contact between particles.

The insertion of lithium into the A-*LFP* structure actually occurs in two separate intercalation plateaus, at 2.85 and 2.70 V for $0 \le x \le 1$ and $1 \le x \le 1.8$, respectively (Fig. 3a). This observation suggests a three-phase mechanism with the existence of an intermediate composition at $x = 1$ ($Li_4Fe_2(PO_4)_3$) and of a final composition at $x = 2$ ($Li_5Fe_2(PO_4)_3$). To check this assumption, chemical lithiation of $Li_3Fe_2(PO_4)_3$ powders was performed with different amounts of *n*-butyllithium in hexane solution. The XRD patterns of the lithiated $Li_{3+x}Fe_2(PO_4)_3$ solids ($0 \le x \le 1.5$) remain essentially similar to one another; peak intensity changes suggest different lithium distributions in the interstitial space at intermediate compositions, leaving the $[Fe_2(PO_4)_3]_\infty$ framework unchanged.

Figure 4 shows the discharge–charge curves obtained at 0.1 mA/cm^2 for the isotypic composition $Li_3Fe_2(AsO_4)$ (A-*LFA*). A same number of lithium ions could be intercalated ($x \sim 1.8$) in a similar fashion as in A-*LFP*. Two intercalation plateaus are still observed at slightly different potentials: 2.90 and 2.60 V for $0 \le x \le 1$ and $1 \le x \le 1.8$, respectively. Whether the $(XO_4)^{3-}$ polyanion contains P or As seems, therefore, to have only a small influence on the position of the redox potential of the Fe^{3+}/Fe^{2+} couple. Phosphorus and arsenic have very similar electronegativities: the inductive effect on the Fe–O bond strength and therefore on the energy position of the Fe^{3+}/Fe^{2+} redox couple in A-*LFX* is essentially unchanged.

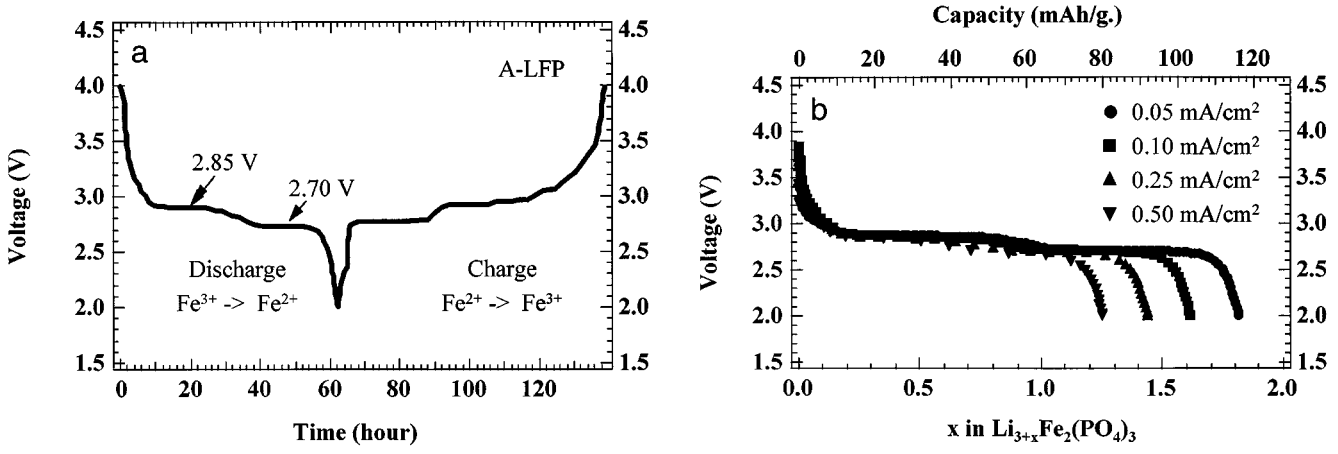

FIG. 3. Electrochemical characteristics of A-*LFP*: (a) discharge–charge curves for the first cycle at 0.1 mA/cm^2; (b) discharge curves at different current densities.

B. "NASICON" $Li_{3+x}Fe_2(PO_4)_3$ (B-LFP)

Intercalation of lithium into the rhombohedral NASICON structure proceeds reversibly (Fig. 5) for approximately $0 \leq x \leq 1.8$, but in a manner quite different from that for A-*LFP*. Although the average V_{oc} ($\sim$2.75 V) remains unchanged from one structure to the other, the shape of the charge and discharge curves is quite altered. Unlike A-*LFP*, there are no distinct plateaus on either the discharge or charge curves for B-*LFP*, suggesting that the insertion/extraction proceeds as in a solid solution. In contrast with what was observed for A-*LFP*, there is no separation of distinguishable Fe^{3+}/Fe^{2+} redox energies for B-*LFP* through the whole intercalation process.

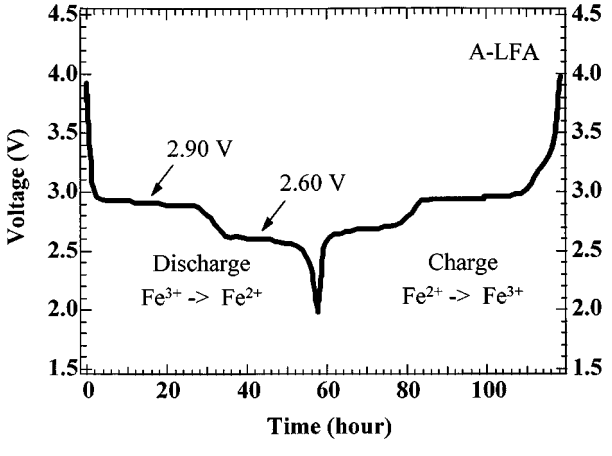

FIG. 4. Electrochemical discharge–charge curves of A-*LFA* curves for the first cycle at 0.1 mA/cm^2.

Up to 2 lithium ions per formula unit can be inserted into $Li_3Fe_2(PO_4)_3$, leading to $Li_5Fe_2(PO_4)_3$: it is well known that the NASICON solid solution $Na_{1+x}Zr_2Si_xP_{3-x}O_{12}$ first described by Hong (22) extends to $x = 3$, at which composition both the Na(1) and Na(2) crystallographic sites are totally occupied. It is therefore surprising to observe a complete solid-solution type behavior for the intercalation of lithium up to $Li_5Fe_2(PO_4)_3$. Although the NASICON framework remains unchanged on passing from B-*NFP* to B-*LFP* and then to $Li_5Fe_2(PO_4)_3$, lithium-ion distributions may differ quite a lot. Powder neutron diffraction experiments will be performed in the near future to fully characterize the lithium-ion distributions in $Li_{3+x}Fe_2(PO_4)_3$ ($0 \leq x \leq 2$).

Another difference in the electrochemical properties of B-*LFP* as compared to A-*LFP* is the smaller capacity loss as the current is increased from 0.05 to 0.5 mA/cm^2 (Fig. 5b and Fig. 6). These electrochemical tests were performed on A-*LFP* and B-*LFP* cathode pellets having the same mass of active material. A reversible discharge capacity of 95 mA h/g is still observed for B-*LFP* at 20 mA/g, a performance that may be directly related to the difference in lithium-ion conductivity between A-*LFP* and B-*LFP*. As pointed out in the previous section, the capacity fade is essentially due to a kinetic effect rather than to a loss of electrical contact between *LFP* particles. The rhombohedral framework of the NASICON structure in B-*LFP* allows for a faster ionic transport and hence for higher performance at high current densities.

Such a reasonably good response of the NASICON B-*LFP* structure to high current densities prompted us to perform cyclability tests in Li/$LiClO_4$(PC–DME)/B-*LFP* coin cells (Fig. 7). With a current density of 23 mA/g (or 1 mA/cm^2), the initial capacity of 95 mA h/g is maintained up to the 40th cycle.

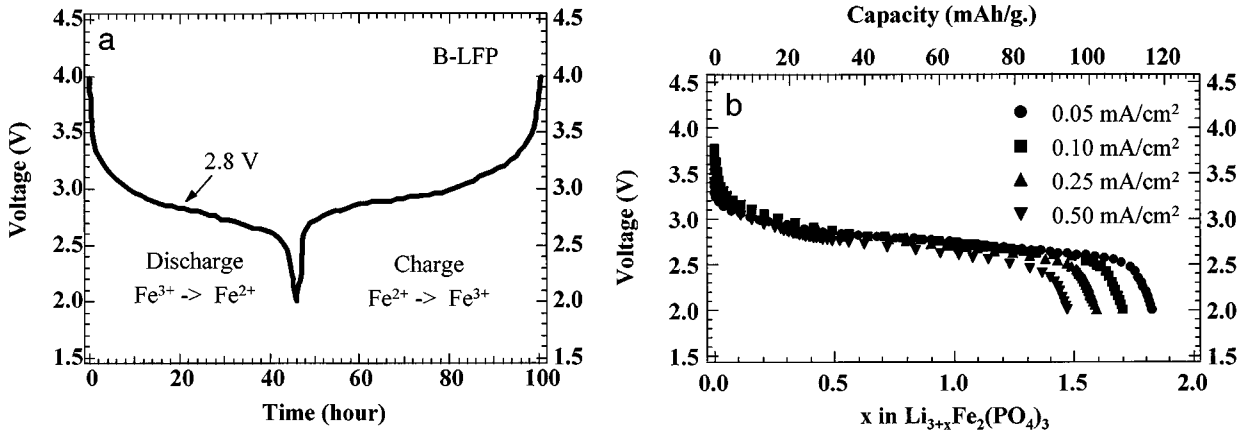

FIG. 5. Electrochemical characteristics of B-*LFP*: (a) discharge–charge curves for the first cycle at 0.1 mA/cm^2; (b) discharge curves at different current densities.

C. "Form II" $Li_3Fe_2(AsO_4)_3$ (C-LFA)

The insertion/extraction of lithium into/from C-*LFA* provides an additional demonstration of the influence of the polyanion and of the crystal structure on the electrochemical properties of the different $Li_3Fe_2(XO_4)_3$ polymorphs.

The first discharge–charge cycle of C-*LFA*, obtained at 0.1 mA/cm^2 (Fig. 8), reveals a reversible insertion of lithium. The shape of the V_{cc} vs composition curves, however, differs qualitatively from discharge to charge, suggesting an irreversible structural change on the first cycle. On the other hand, subsequent cycles are reversible, the shape of the curves being that of the first charge. The total number of lithium ions that can be electrochemically inserted into the II-$Li_3Fe_2(AsO_4)_3$ structure is approximately equal to 1.5, for a capacity of 80 mA h/g. The first discharge curve consists of two separate domains with a plateau at 3.1 V vs lithium ($0 \leq x \leq 0.5$) and a continuous voltage decrease between 2.5 and 2 V in the range $0.5 \leq x \leq 1.5$.

The existence of a first intercalation plateau suggests the formation of an intermediate, well-defined composition of stoichiometry $Li_{3.5}Fe_2(AsO_4)_3$ (i.e., $Li_7Fe_4(AsO_4)_6$) analogous to the "nonstoichiometric" II-*NFA* crystals prepared under reducing conditions with general formula $Na_7Fe_4(AsO_4)_6$ (24, 25): the total occupancy of the Na(2) site is compensated by the reduction of one-fourth of the iron, which actually occurs on the central Fe(1) site. The relatively high V_{oc} may be accounted for by the greater volume per formula unit (hence smaller Madelung energy) of C-*LFA* (247.8 Å^3) compared with A-*LFA* (235.7 Å^3). It may also be understood in terms of different local environments around $Fe(1)O_6$ and $Fe(2)O_6$ octahedra, as recently pointed out by Padhi *et al.* (15) on comparing Fe^{3+}/Fe^{2+} redox couple energies in the phosphates $LiFePO_4$, $LiFeP_2O_7$,

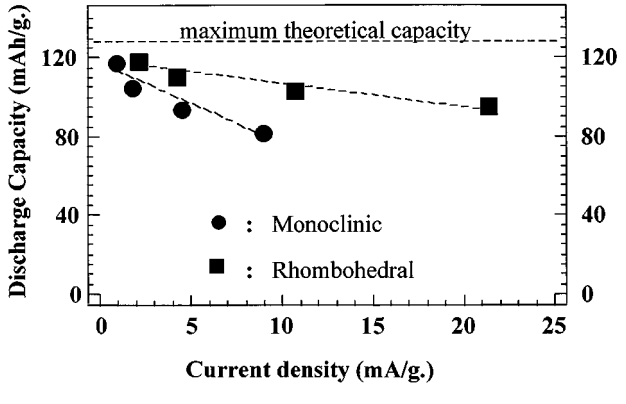

FIG. 6. Comparison of capacities at various current densities for the two $Li_3Fe_2(PO_4)_3$ polymorphs A-*LFP* and B-*LFP*.

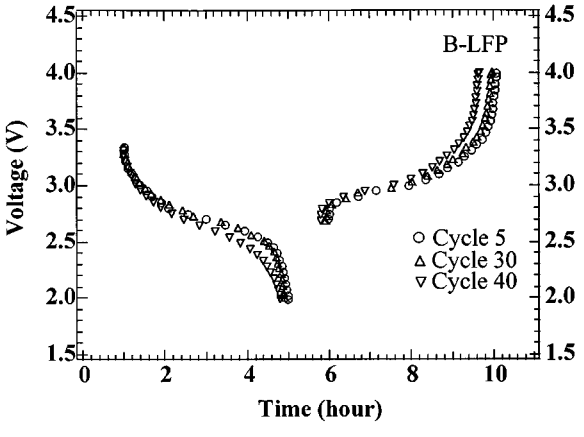

FIG. 7. Electrochemical cycling of B-*LFP* at 1 mA/cm^2.

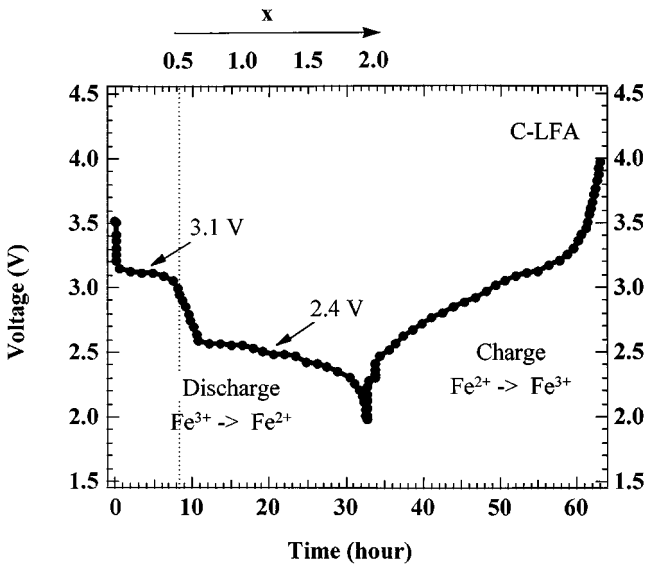

FIG. 8. Electrochemical discharge–charge curves of C-*LFA* for the first cycle at 0.1 mA/cm^2.

$Fe_4(P_2O_7)_3$, and $Li_3Fe_2(PO_4)_3$. Extensive edge-sharing between FeO_6 octahedra in the olivine $LiFePO_4$ lowers the Madelung energy, which lowers the energy of the Fe^{3+}/Fe^{2+} redox couple and thus generates a much higher open-circuit voltage (3.5 V vs Li) than is found in NASICON-type phosphates (2.8 V vs Li). In C-*LFA*, the $Fe(1)O_6$ octahedron shares three of its edges with $Fe(2)O_6$ octahedra. Each $Fe(2)O_6$ octahedron, in turn, shares only one edge with the central $Fe(1)O_6$ octahedron. Consequently, the electric field at the Fe(1) position is smaller than that at the Fe(2) site, so the Fe(1) positions are the first to be reduced. The extra lithium atoms that can be inserted into the structure apparently force a rearrangement of the Li^+ ions in the interstitial space, and the original distribution is not recovered at room temperature on recharge. Disorder of the Li^+ ions leads to a higher Li^+-ion mobility.

IV. CONCLUSION

The four $Li_3Fe_2(XO_4)_3$ (X = P or As) polymorphs described in this paper show interesting properties of reversible intercalation/extraction of lithium corresponding to the reduction–oxidation of Fe^{3+}/Fe^{2+} at $2.5 \leq V_{oc} \leq 3$ V vs lithium. The position of the Fe^{3+}/Fe^{2+} redox couple below the Fermi energy of the lithium anode is nearly independent of the crystal structure and whether X = P or As. There is, however, a clear dependence of (i) the shape of the V_{oc} vs x curves for $Li_{3+x}Fe_2(XO_4)_3$ and (ii) the charge–discharge rate capabilities on the crystal structure of the cathode material.

Monoclinic $Fe_2(SO_4)_3$-type A-*LFX* (X = P, As) show distinct intercalation plateaus at voltages ranging between 2.9 and 2.6 V with the probable existence of a well-defined intermediate composition $Li_4Fe_2(XO_4)_3$. A two-phase interface results in a diffusion-limited deintercalation–intercalation process responsible for a poor response at high current densities. Additionally, we found that the position of the Fe^{3+}/Fe^{2+} redox couple in $Li_{3+x}Fe_2(XO_4)_3$ ($\sim$2.8 eV below the Fermi energy of Li) was essentially unchanged between A-*LFP* and A-*LFA* due to the very similar electronegativities of P and As.

The rhombohedral NASICON B-*LFP*, on the other hand, shows promising performances due to a more open framework allowing fast diffusion of lithium ions. The intercalation of lithium into the rhombohedral form of $Li_{3+x}Fe_2(PO_4)_3$, $0 \leq x \leq 2$, was demonstrated for the first time. It proceeds with a continuous decrease of the cell voltage between 3 and 2.5 V vs lithium for a discharge capacity of 115 mA h/g at 0.1 mA/cm^2. The response to high current densities is definitely improved for B-*LFP*, where much smaller capacity loss is observed than for A-*LFP*.

Finally, we showed that a third polymorph of general formula $Li_{3+x}Fe_2(AsO_4)_3$, C-*LFA*, with a rhombohedral "cluster-type" structure could also reversibly intercalate lithium between 3.2 and 2.5 V vs Li. In that case, however, distinct environments around the two kinds of FeO_6 octahedra result in distinct values of the Fe^{3+}/Fe^{2+} redox couple, at 3.1 and 2.7 V vs Li for Fe(1) and Fe(2), respectively.

ACKNOWLEDGMENTS

The Robert A. Welch Foundation (Houston, TX) and the Institute for Advanced Technology, University of Texas at Austin, federated with the U.S. Army Research Laboratory are acknowledged for financial support.

REFERENCES

1. A. Nadiri, C. Delmas, R. Salmon, and P. Hagenmuller, *Rev. Chim. Miner.* **21,** 537 (1984).
2. W. M. Reiff, J. H. Zhang, and C. C. Torardi, *J. Solid State Chem.* **62,** 231 (1986).
3. C. C. Torardi and E. Prince, *Mater. Res. Bull.* **21,** 719 (1986).
4. A. Manthiram and J. B. Goodenough, *J. Solid State Chem.* **71,** 349 (1987).
5. C. Delmas, F. Cherkaoui, A. Nadiri, and P. Hagenmuller, *Mater. Res. Bull.* **22,** 631 (1987).
6. C. Delmas, A. Nadiri, and J. L. Soubeyroux, *Solid State Ionics* **28–30,** 419 (1988).
7. A. Manthiram and J. B. Goodenough, *J. Power Sources* **26,** 403 (1989).
8. S. Okada, K. S. Nanjundaswamy, A. Manthiram, and J. B. Goodenough, *Proc. 36th Power Sources Conf.*, Cherry Hill, NJ, June 6–9, 1994.
9. K. S. Nanjundaswamy, A. K. Padhi, and J. B. Goodenough, *Solid State Ionics* **92,** 1 (1996).
10. P. C. Christidis and P. J. Rentzeperis, *Z. Kristallogr.* **141,** 233 (1975).
11. P. C. Christidis and P. J. Rentzeperis, *Z. Kristallogr.* **144,** 341 (1976).
12. A. K. Padhi, K. S. Nanjundaswamy, and J. B. Goodenough, *Proc. 189th ECS Meeting*, Los Angeles, CA, May 1996.

13. A. K. Padhi, K. S. Nanjundaswamy, C. Masquelier, and J. B. Goodenough, *Proc. 37th Power Sources Conf.*, Cherry Hill, NJ, June 17–20, 1996.
14. C. Masquelier, A. K. Padhi, K. S. Nanjundaswamy, S. Okada, and J. B. Goodenough, *Proc. 37th Power Sources Conf.*, Cherry Hill, NJ, June 17–20, 1996.
15. A. K. Padhi, K. S. Nanjundaswamy, S. Okada, C. Masquelier, and J. B. Goodenough, *Proc. 190th ECS Meeting*, San Antonio, TX, October 1996.
16. C. Masquelier, K. S. Nanjundaswamy, A. K. Padhi, and J. B. Goodenough, *Proc. 190th ECS Meeting*, San Antonio, TX, October 1996.
17. M. Pintard-Scrépel, F. d'Yvoire, and F. Rémy, *C. R. Acad. Sci. Paris* **286,** 381 (1978).
18. F. d'Yvoire, M. Pintard-Scrépel, E. Bretey, and M. de la Rochère, *Solid Statie Ionics* **9&10,** 851 (1983).
19. F. d'Yvoire, M. Pintard-Scrépel, and E. Bretey, *Solid State Ionics* **18&19,** 502 (1986).
20. J. M. Winand, A. Rulmont, and P. Tarte, *J. Solid State Chem.* **87,** 83 (1990).
21. A. B. Bykov, A. P. Chirkin, L. N. Demyanets, S. N. Doronin, E. A. Genkina, A. K. Ivanov-Shits, I. P. Kondratyuk, B. A. Maksimov, O. K. Mel'nikov, L. N. Muradyan, V. I. Simonov, and V. A. Timofeeva, *Solid State Ionics* **38,** 31 (1990).
22. Hong, H. Y. P., *Mater. Res. Bull.* **11,** 173 (1976).
23. H. Schwarz and L. Schmidt, *Z. Anorg. Allg. Chem.* **387,** 31 (1972).
24. F. d'Yvoire, E. Bretey, and G. Collin, *Solid State Ionics* **28–30,** 1259 (1988).
25. C. Masquelier, F. d'Yvoire, and G. Collin, *J. Solid State Chem.* **118,** 33 (1995).